Fabrication of PEM Fuel Cell Bipolar Plates by Indirect SLS

Ssuwei Chen, David L. Bourell, Kristin L. Wood
Department of Mechanical Engineering, Laboratory for Freeform Fabrication
The University of Texas at Austin, Austin, Texas, 78712

Abstract

The paper presents a new manufacturing technique involving Selective Laser Sintering (SLS) for proton exchange membrane fuel cell (PEMFC) bipolar plate fabrication. A material system for bipolar plate fabrication was identified to satisfy both the cell performance requirement and SLS operation restriction. Carbonization and liquid epoxy infiltration are subsequently performed following the completion of SLS green bipolar plate. The finished SLS bipolar plate showed impressive surface finish and mechanical strength, and a single fuel cell was assembled with two SLS end plates and membrane electrode assembly (MEA) in between. Various physical property tests were performed with positive results. Fuel cell performance (voltage vs. current density, voltage vs. time, etc.) will be assessed in the near future.

1. Introduction

Bipolar plates, most fabricated by machining of pure graphite, are one of the most expensive components in proton exchange membrane fuel cells (PEMFC). Extreme care must be taken during the costly and time-consuming machining process, mainly because of the brittleness of graphite. The layer-based nature of selective laser sintering (SLS) offers several advantages for bipolar plate development and manufacturing. This additive process possesses the ability to manufacture complex geometries that are otherwise difficult to obtain, among which are the grooved flow fields on both sides of bipolar plates. Furthermore, integrated cooling channels reserved for improving thermal management, can be simultaneously formed on the central surfaces of the plate rather than by gluing two half plates back-to-back as is used in many other techniques. Even though application of SLS for bipolar plate fabrication may not be suitable for mass volume production at present, it will significantly benefit research in fuel cell flow field design since prototypes can be done in a much shorter period of time compared to traditional machining.

244

2. Requirements for Bipolar Plate

An optimized bipolar plate has to fulfill several requirements to maximize cell performance. From the material point of view, high electric conductivity could minimize the ohmic losses, meaning that voltage drop across the bipolar plate can be reduced. Even though it is always desirable to obtain plate materials with low bulk resistivity so as to reduce the voltage loss, it has been shown that the potential drop across the plate/electrode interface is many orders of magnitude more than that across the bipolar plate itself [1]. Therefore, finding a material more electrically compatible with the electrode material plays a more important role from the viewpoint of minimizing overall potential losses.

Bipolar plates also require very low gas permeability with respect to reactant gases. Since hydrogen and air/oxygen are flowing in the flow fields on opposite sides of the bipolar plate, it is important to make sure that both gases are not mixed by permeation through the plate. Gas tightness of the bipolar plate not only prevents the cross leaks of reactant gases, but also removes the possibility of dangerous gas leakage into the exterior fuel cell environment. As far as safety and fuel saving are concerned, bipolar plates with a high gas impermeability are a top priority.

Both heat and water/vapor are byproducts of the PEM fuel cell net reaction. Bipolar plate materials having a high thermal conductivity are desired to make best use of the produced heat. The overall fuel cell efficiency could be boosted up to 70% [2] if most of the heat can be cycled. With high thermal conductivity, the bipolar plate is able to transfer heat efficiently to the designed heat exchange unit and maintain the system temperature in the operating range. This is especially important in automotive applications since heat produced can be treated as the source of energy for the heating units. Additionally, high heat conductivity also ensures low temperature gradients in bipolar plate and eliminates the possible thermal strains and stresses.

Corrosion resistance and chemical stability are the two other properties important for bipolar plates. PEM fuel cell bipolar plates are generally in contact with an acidic MEA and operate in a hot and humid environment [3]. Without a certain level of resistance to corrosion, a bipolar plate would oxidize and corrode easily during its long-term lifetime. Corroded bipolar plates can no longer provide the standard mechanical

strength and may form contamination in the MEA membrane, resulting in the degradation of fuel cell performance [4].

In addition, bipolar plates need to be slim and light to keep the stack volume and weight low. Low density plate materials satisfy these requirements. Many electrochemical parameters, such as volumetric power, volumetric energy and gravimetric capacity, etc., can be increased dramatically by using low specific weight materials. Finally, the cost of both bipolar plate material and manufacturing technique needs to be lowered to promote commercialization of PEM fuel cells. PEM fuel cells currently are prohibitively expensive, due significantly to bipolar plate cost [5]. Thus, searching for an inexpensive bipolar plate material with the capability for easy fabrication has become the major task for industries that are trying desperately to make commercial PEM fuel cells.

3. Material Selection and Manufacturing Procedures

3.1 Material Selection and Screening Test

A material system was chosen consisting of graphite as the matrix material and phenolic as the binder. Phenolic is well known for giving excellent bonding strength upon curing and more importantly, a higher carbon yield can be obtained when complete carbonization is performed [6]. Table 1 lists a comparison of carbon yield from some selected hydrocarbon polymers.

Material	Theoretical carbon Content (%)	Carbon yield (%) after Pyrolysis
Phenolic resin	<80	55-70
Furan resin	<75	50-60
Epoxy resin	<75	20-30
Unsaturated polyester resin	<60	15-25

Table 1 Carbon yield for selected materials

The nature of graphite makes it an excellent choice for bipolar plate fabrication as far as material requirements are concerned. However, extremely poor wettability and surface roughness render it relatively unfit for processing using powder metallurgy. Wettability of graphite powder plays a very important role in this case since phenolic resin, which serves as the binder, is expected to be fused into a preform in the liquid phase to provide the initial binding strength between graphite particles during sintering.

246

The strategy to overcome the low wettability barrier is to mix finer particle size phenolic resins with relatively coarser pure graphite particles. It is expected that a large amount of phenolic resin powder will become uniformly dispersed over the larger graphite particle surfaces, which will facilitate better binder flow during sintering and promote the binding strength. Increased binder level is advantageous to increased green strength; however, more geometric shrinkage occurs accompanying this. There should be a compromise as these two issues are considered. Figure 1 shows a mixture of phenolic and graphite powders in which finer phenolic resins are scattered over the coarser graphite powders.
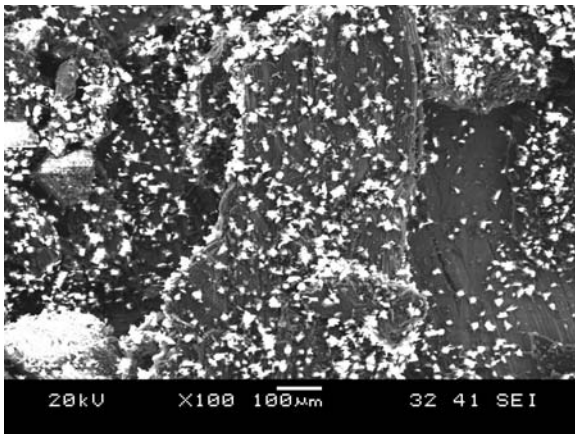
Fig.1 Roller mixed mixture of graphite
   and phenolic powders

Packing of powder is closely related to the green part density and hence, green strength. Particle size and particle shape are the two dominant factors influencing the efficiency of powder packing [7]. The amount of friction of a powder increases as its surface area increases. More friction between particles results in less efficient flow and packing [8]. As shown in Figure 2, graphite particles are quite irregular and flaky in shape and rough on the surface, which make it hard to be compacted acceptably. One way to reduce the friction between particles is to use graphite powders coarser in size since most fine powders will not flow because of their high inter-particle friction. Adjustment of particle size distribution may be beneficial for more compact packing of powders as well. Packing efficiency can be improved by mixing selective sizes so as to fill interstices between particles.
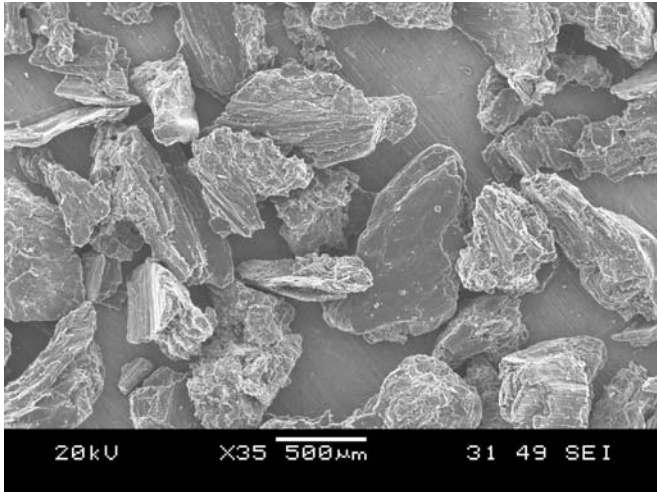
Fig. 2 SEM of pure graphite particles

However, too wide a distribution of particle size increases the net surface area so that poor packing results. The optimized size distribution was initially screened for better powder flow and surface finishing of the parts. Three groups of graphite powders were obtained commercially and some of their physical properties are summarized in Table 2. The BET surface area was measured by a Micromeritics ASAP 2010 Surface Area Analyzer.

Source of graphite powder	Theoretical Density (g/cm^3)	Apparent Density (g/cm^3)	Size Distribution	BET Surface Area (m^2/g)
GrafTech (GP44R)	2.25	0.254	90% < 41 μm 50% < 18 μm	11.35
GrafTech (GS150E)	2.24	0.35	90% < 100 μm 50% < 55 μm	4.03
Alfa Aesar (Stock#43816)	2.25	---	-50~140 mesh (105~297 μm)	1.25

Table 2 Properties of graphite powder examined

A screening test was executed with a high temperature furnace to make bar-shape samples and their mechanical strength and surface smoothness were evaluated. Eventually, GrafTech GS150E graphite powder was chosen for the material system with a combination of at least 25% to 30% phenolic resin powder obtained from Georgia Pacific Resins, Inc. The phenolic powder was 31 μm initially but was ground in HJE Company, Inc. to a final size of 11 μm.

3.2 SLS of Green Bipolar Plate

The roller mixed graphite and phenolic powder were subsequently loaded into a SinterStation 2000 SLS machine to build green bipolar plates. Curling took place during green part formation. This unwanted effect can be mitigated through bulk powder bed temperature control. In the direct SLS processes, powder bed temperature is usually raised up to a point close to the fusing point of sintering material so as to minimize the thermal gradient [9, 10]. However, in indirect SLS processes involving multiple material constituents, this strategy is difficult to fulfill especially for graphite having high melting point and a thermosetting material, phenolic. Figure 3 shows the DSC curve for phenolic resins. A powder bed temperature of 55ºC was chosen since almost no critical thermodynamic events took place until around this point during the irreversible curing process. The first endothermic peak corresponds to melting of novolac resin while the second broad peak corresponds to heat of solution of hexamine in the molten resin [11]. The only exothermic peak in the graph represents the cross-linking mechanism of novolac resin and hexamine, which occurs at around 150ºC. In addition, a laser power of 14 watts, a laser scan spacing of 0.003 inch and a layer thickness of 0.004 inch were used to produce optimum plate quality.
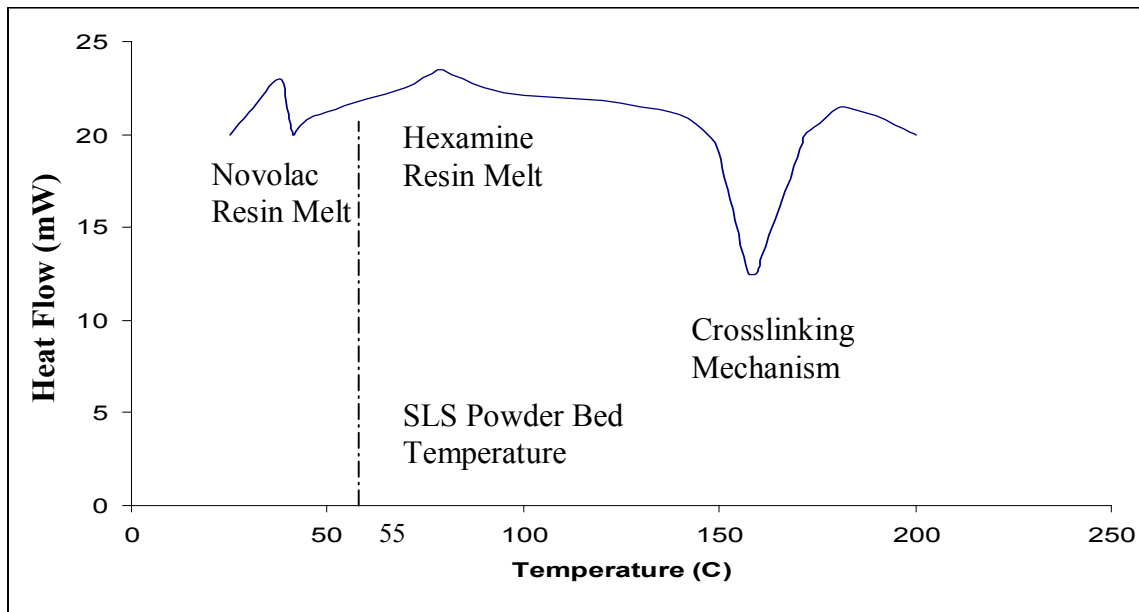

Fig. 3 DSC curve for phenolic resin

3.3 Carbonization and Post Processing

Parts produced from SLS are expected to be more porous, weaker and lower in conductivity compared to machined bipolar plates from bulk graphite. Post processing then would be required to densify the part and attain gas impermeability. The finished green bipolar plate was removed from the powder cake, and loose powders were brushed off before loading it into a high temperature, vacuum furnace and converting the phenolic resin into carbon residue [12]. The carbonized phenolic resin exhibits an amorphous, glass-like structure as can be verified by XRD pattern shown in Figure 4. The curing process was done in a reducing environment by filling the vacuum chamber with either argon or nitrogen forming gas to ensure that a maximum amount of carbon residue was left during the carbonization. To prevent curling of brown parts during carbonization, the bipolar plates were all sandwiched by two pieces of graphite slabs during curing. However, some dimensional reduction became more visible in the vertical z-direction since the weight of graphite slabs made the parts even more compact.
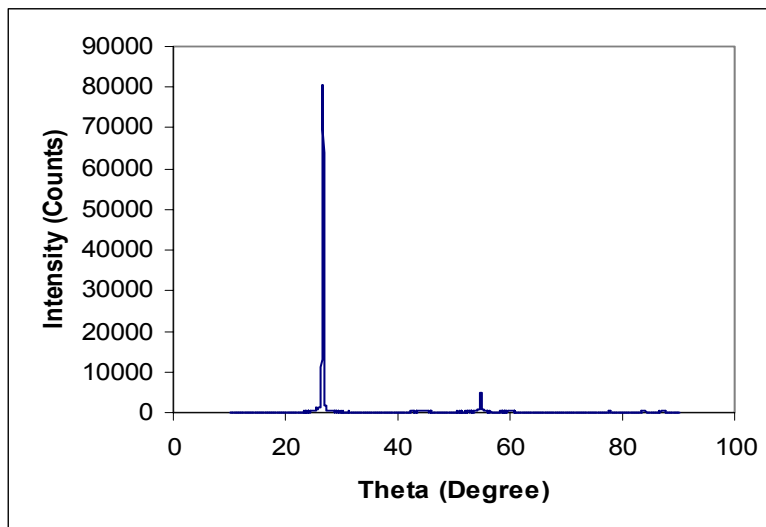
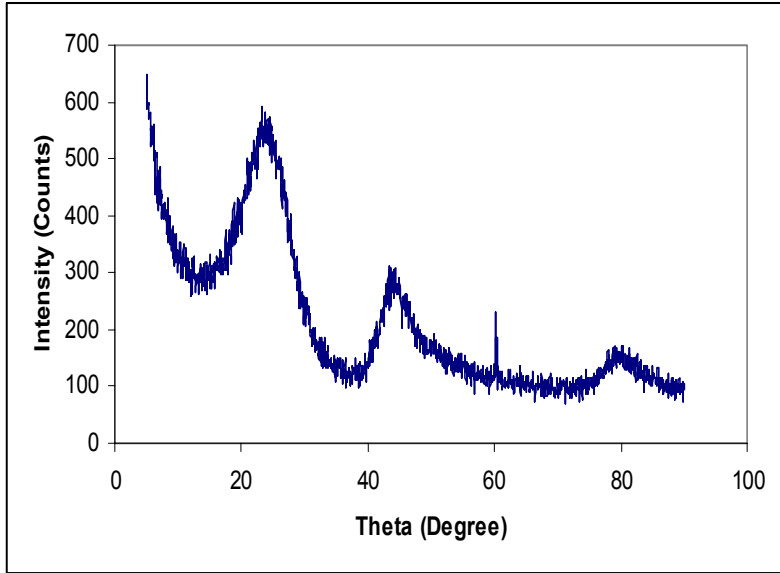Fig. 4(a) Xray diffraction pattern of GS 150E graphite powder

250

Fig. 4(b) Xray diffraction pattern of carbonized phenolic resin, revealing the amorphous crystal structure

Upon completion of the curing cycle, the cured brown bipolar plates were cooled and immersed in liquid epoxy resin for a period of a couple of minutes, depending on the viscosity of the resin used [13], to make the porous structure gas tight. The liquid epoxy resin intruded into open pores of the brown part without producing noticeable dimensional change to the part. Solvents, such as toluene or xylene, were required to dilute the as-received liquid epoxy resin since most are too viscous to penetrate into the graphite pore structure. During infiltration, gas bubbles kept coming out of the part surfaces, indicating the porous structures were being filled by epoxy resin due to the capillary forces. Infiltration of at least two times was needed to create a completely gas tight plate surface. Infiltrated bipolar plates were subsequently oven dried at 60° C to speed up the curing process. Figure 5 shows SEM micrographs of the plate surface taken from different stages during fabrication procedures.
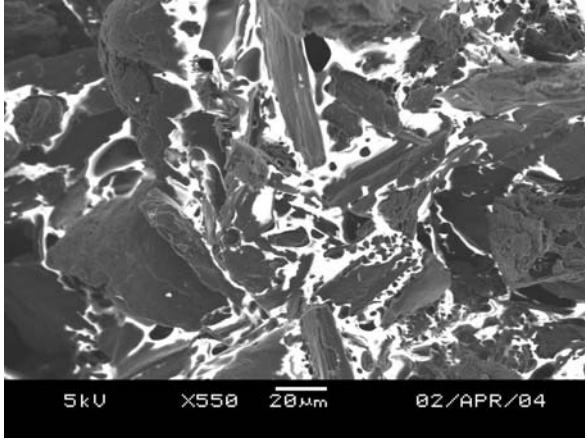
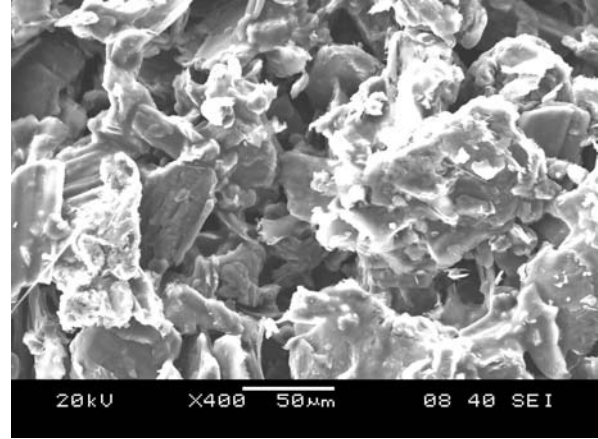Fig. 5(a) Green part micrograph after SLS

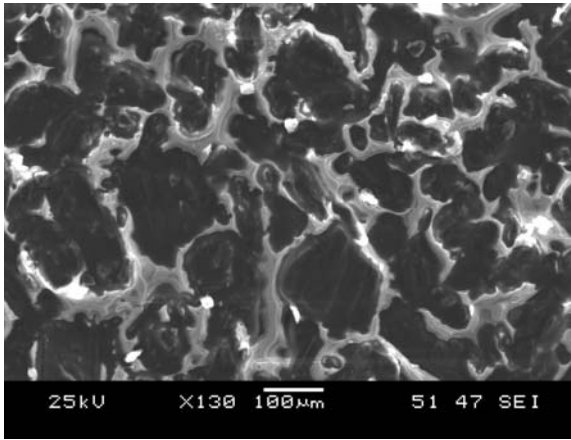Fig. 5(b) Brown part micrograph after phenolic burnout

Fig.5(c) Infiltrated part micrograph

Figure 5(a) presents the microstructure of green part. As can be seen, the phenolic resin provides bonding between graphite powders with significant porosity. This bonding could be adjusted through binder level optimization to give the adequate green strength for basic plate handling during post processing. Figure 5(b) demonstrates the cured brown part structure details. More open and interconnected pores can be observed due to the burning-off of the phenolic resin, and most of the resin residue was converted into carbon. The curing process at this stage boosted the electrical conductivity dramatically as well as mechanical strength compared to the green part, which may partially be explained by the reduction of porosity in the part [14, 15]. In Figure 5(c), after epoxy infiltration, most of the pores were filled up, giving rise to a much more hermetic surface finish. Moreover, the infiltrated parts were not inferior to brown parts in electrical conductivity based on two point probe ohmic testing, indicating that the overall carbon phases, inclusive of graphite and converted phenolic resin, are interconnected to each other without interruption by the insulating epoxy resin.

4. Electrical and Physical Property Testing

Bulk electric conductivity was measured by four point probe technique, which is commonly used because of its ability to eliminate the contact resistance between the probe and test sample. Flexural strength was obtained by three point bend testing (ASTM D790) on a rectangular bar having exactly the same composition as the finished bipolar plate. A Quantachrome ultrapycnometer was used to measure the density of the plate and corrosion rate was measured electrochemically by a potentiostat. A 0.01 M HCl + 0.01 M Na_2SO_4 solution was used in corrosion test to mimic the real fuel cell operating environment [3]. Lastly, a Varian Portatest helium gas leak detector was used to evaluate the gas impermeability. These properties are summarized and compared with some selected novel bipolar plates in Table 3. A single PEM fuel cell assembled by two SLS end plates along with one end plate are shown in Figure 6(a) and two 3 mm thick SLS bipolar plates are shown in Figure 6(b).

Type \\ Property	Department of Energy (DOE)Target Value	IGT (molded graphite composite bipolar plate) [16]	Oak Ridge National Lab/ Porvair Fuel Cell Technology (slurry molding of carbon/carbon composite bipolar plate) [17, 18, 19]	SLS Bipolar Plate
Flexural Strength(psi)	> 600	>3000	4200	>1730
Electric Conductivity(S/cm)	>100	250~350	200~300	80
Specific Weight (g/cm^3)	---	---	1~1.3	1.27
Corrosion Rate ($\mu A/cm^2$)	< 16	< 5	6	< 9
Gas Permeability (cm^3/cm^2-s)	<16x10^{-6}	< 2x10^{-6}	< 2x10^{-6}	5x10^{-6}

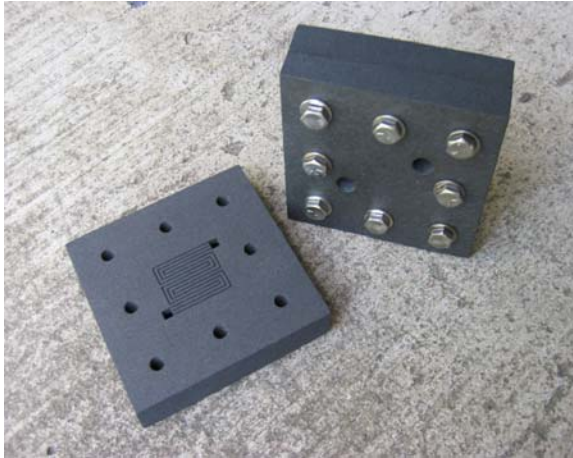Table 3 Property of SLS and selected molded bipolar plates

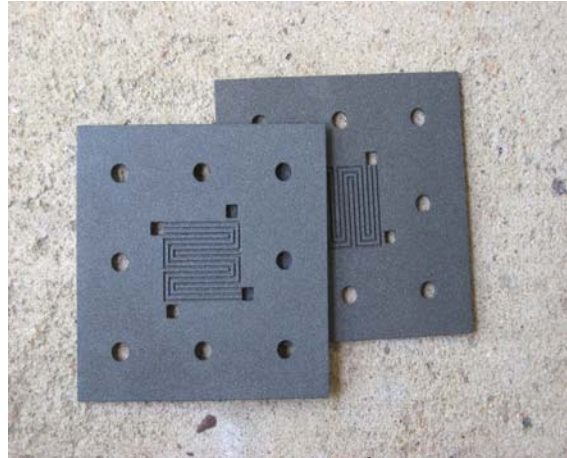Fig. 6(a) One end plate on the left and a stack assembly on the right

Fig. 6(b) Two 97x97x3 mm^3 bipolar plates with 8.5 cm^2 active area each

5. Discussion and Conclusion

The work done so far shows the feasibility of application of SLS to fuel cell bipolar plate fabrication. The properties of SLS graphite composite plates are promising and both the material and process costs are reduced compared to traditional machining of pure graphite. However, the dimensional shrinkage during brown part formation posed a challenge as far as geometric accuracy is concerned. Fortunately, the dimensional reduction can be compensated by scaling up the initial plate design since the shrinkage seems to be linear if the powders are well mixed and no density gradient exists in the batch. Finally, single fuel cell polarization curve and contact resistance between bipolar plate and MEA will be measured to justify the cell performance. The overall manufacturing procedure is given in Figure 7.
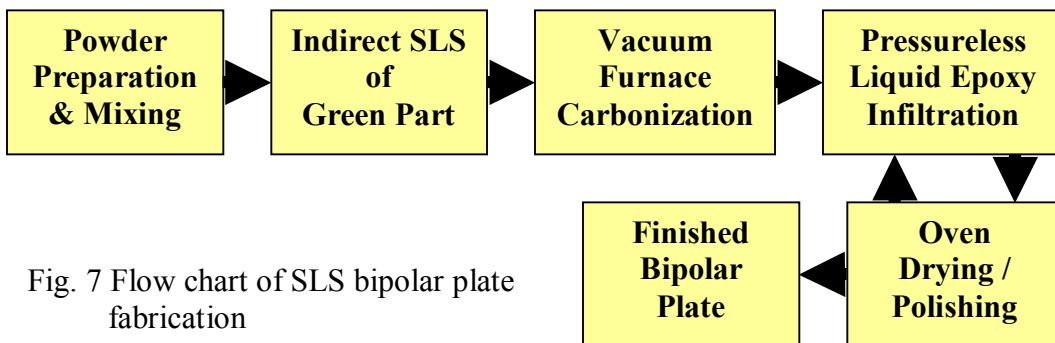

Fig. 7 Flow chart of SLS bipolar plate fabrication

Powder Preparation & Mixing → Indirect SLS of Green Part → Vacuum Furnace Carbonization → Pressureless Liquid Epoxy Infiltration → Oven Drying / Polishing → Finished Bipolar Plate

References

[1] E. J. Carlson, N. Garland, R. D. Sutton, Cost Analyses of Fuel Cell Stack/Systems Available at http://www.eere.energy.gov/hydrogenandfuelcells/pdfs/iva3_carlson.pdf

[2] J. Larminie, Fuel Cell Systems Explained, 2nd ed. / Chichester, West Sus / 2003

[3] M. Li, S. Luo, C. Zeng, J. Shen, H. Lin, C. Cao, Corrosion behavior of TiN coated type 316 stainless steel in simulated PEMFC environments, Corrosion Science, 2003

[4] R. Makkus, A. Janssen, F. Bruijn, R. Mallant, J. Power Sources 86 (2000) 274-282

[5] H. Tsuchiya, O. Kobayashi, Inter. J. Hydrogen Energy 2003

[6] A. Gardziella, L. A. Pilato, A. Knop, Phenolic resins, 2nd ed./Springer

[7] R. M. German, Powder Metallurgy Science, MPIF/ Princeton, New Jersey

[8] C. Selcuk, R. Bentham, N. Morley, J. V. Wood, Powder Metallurgy, Vol. 46 No. 2 (2003)117-120

[9] P. Calvert, R. Crockett, J. Lombardi, J. O'Kelly, K. Stuffle, Proceedings of the Solid Freeform Fabrication Symposium, August 8-10, 1994

[10] C. Amon, J. Beuth, H. Kirchner, R. Merz, F. Prinz, K. Schmaltz, L. Weiss, Proceedings of the Solid Freeform Fabrication Symposium, August 9-11, 1993

[11] R. Burns, E. W. Orrell, J. Materials Science, 2 (1967) 72-77

[12] G. Bhatia, R. K. Aggarwal, M. Malik, O. P. Bahl, J. Materials Science, 19 (1984) 1022-1028

[13] A. G. Kostornov, Powder Metallurgy and Metal Ceramics, Vol. 42 Nos. 9-10 (2003)

[14] J. M. Montes, J. A. Rodriguez, E. J. Herrera, Powder Metallurgy, Vol. 46 No. 3 (2003)

[15] O. F. Boitsov, L. I. Chernyshev, V. V. Skorokhod "Effects of Porous Structure on The Electrical Conductivity of Highly Porous Metal-Matrix Materials", Powder Metallurgy and Metal Ceramics, Vol. 42 Nos. 1-2 (2003)

[16] Fuel Cell for Transportation Contractor's Annual Progress Report. Available at http://www.ott.doe.gov/pdfs/contractor.pdf

[17] ORNL report. Available at http://www.pnl.gov/microcats/ottreview/ottmeeting/14-Besman.pdf

[18] DOE Hydrogen, Fuel Cells & Infrastructure Technologies Program. Available at http://www.eere.energy.gov/hydrogenandfuelcells/pdfs/ive7_haack.pdf

[19] Porvair Fuel Cell Technology. Available at http://www.eere.energy.gov/hydrogenan dfuelcells/pdfs/review04/fc_19_haack_04.pdf

 Acknowledgment